Research Square

Preprints are preliminary reports that have not undergone peer review.
They should not be considered conclusive, used to inform clinical practice,
or referenced by the media as validated information.

Isobavachalcone Activates Antitumor Immunity on Orthotopic Pancreatic Cancer Model: A Screening and Validation

Hongbo Zhang
Tianjin Nankai Hospital
Xuanming Liu
Tianjin University of Traditional Chinese Medicine
Jianlin Cao
Shanxi Provincial People's Hospital
Yuzhen Zhuo
Tianjin Nankai Hospital
Jiahui Jin
Tianjin University of Traditional Chinese Medicine
Qiaoying Gao
Tianjin Nankai Hospital
Xiangfei Yuan
Tianjin Nankai Hospital
Lei Yang
Tianjin Nankai Hospital
Dihua Li
Tianjin Nankai Hospital
Yan Wang (wangyan@tjutcm.edu.cn)
Tianjin University of Traditional Chinese Medicine

Research Article

Keywords: Isobavachalcone, pancreatic cancer, tumor microenvironment, network pharmacology, bioinformatics, molecular docking

Posted Date: April 20th, 2022

DOI: https://doi.org/10.21203/rs.3.rs-1491024/v2

License: This work is licensed under a Creative Commons Attribution 4.0 International License.
Read Full License

Abstract

Pancreatic cancer accompanies poor prognosis and accounts for a significant number of deaths every year. Due to possessing a broad spectrum of bioactivities such as antioxidant and antitumor activity, Psoralea corylifolia L. (PCL) is widely used in clinical Chinese medicine. In the present work, we explored potential antitumor agents of PCL and underlying mechanisms in vivo and vitro experiments. Based on the integration of network pharmacology, protein-protein interaction network, the expression profile of gene, survival analysis, multivariate Cox regression model, and molecular docking, we considered Isobavachalcone (IBC) as a candidate compound. Subsequently, we confirmed that IBC could inhibit Panc 02 cells proliferation and induce apoptosis via increasing ROS production in vitro. Meanwhile, IBC could attenuate the weight of orthotopic pancreatic cancer in mice, increase $CD8^+$ cells and reduce M2 macrophages polarization in the tumor tissue and spleen. IBC also alleviated the proportion of MDSCs in the tumor tissue but had no change in the spleen. In addition, IBC restrained the polarization of RAW 264.7 cells into M2 macrophages by inhibiting the expression of ARG1 and MRC1 and suppressed the expression of ARG1 and TGF-β in BM-derived MDSCs. Thus, IBC can attenuate orthotopic pancreatic cancer growth via activating immune activity and inducing cell apoptosis. This research could be a reference for the antitumor ability of IBC and the treatment of the immunosuppressive tumor microenvironment in pancreatic cancer.

Introduction

Pancreatic cancer, one of the most frequent cancers, is a devastating malignant disease and accounts for at least 331000 deaths every year, which have turned into the seventh highly cause for cancer death (1). Convincing data from the previous study have demonstrated that the present therapeutic options including surgery, radiotherapy, and chemotherapy, only warrant the no more than 9% 5-year survival and 26-month median survival (2, 3). Therefore, it is essential to explore a new therapeutic strategy, such as immunotherapy, to increase the survival rates of pancreatic cancer patients.

Traditionally, pancreatic cancer is considered a "non-immunogenic" tumor, while lately, preclinical data supports that pancreatic cancer can adopt multiple mechanisms to escape immune and form an immunosuppressive microenvironment (4, 5). The section is involved multiple mechanisms, perhaps including the secretion of immunosuppressive chemokines and cytokines, recruiting of regulatory immune cells, and the expression of cell surface proteins (6). Differential immune cell recruitment might act on different roles of immunosuppressive mechanisms in the tumor microenvironment. For example, increased infiltration of T regulatory cells (Tregs), tumor associated macrophage (TAM) with M2 polarization, and myeloid-derived suppressor cells (MDSCs) have been associated with the immune microenvironment of pancreatic cancer and prevented the antitumor activity of effectors $CD4^+$ and $CD8^+$ cells (7). The main feature of these cells is their potent immunosuppressive activity.

Psoralea corylifolia L. (PCL) possesses an excellent efficacy in the treatment of psoriasis and vitiligo and is widely used in clinical Traditional Chinese Medicine (TCM) (8, 9). Due to TCM’s property of multiple

components and targets, it has a broad spectrum of bioactivities, including cytotoxic, antibacterial, antifungal, antitumor, and antioxidant (10). Isobavachalcone (IBC) is firstly extracted from PCL in 1968 and was defined as a prenylated chalcone (11). Previous studies have shown that IBC can inhibit colorectal cancer proliferation, induce apoptosis of prostate cancer PC-3 cells, and promote pro-caspase-3 and pro-caspase-9 in neuroblastoma (12–14). Studies also show that IBC selectively induces leukemic cell death with massive cytoplasmic vacuolation but no impairment to the normal peripheral blood cells (15). These studies indicated that IBC was a promising antitumor agent. However, the level of antitumor ability and underlying molecular mechanisms of IBC against pancreatic cancer remains unclear. We integrated network pharmacology, bioinformatics, and molecular docking to identify a candidate compound and further studied underlying mechanisms. (Fig. 1).

Materials And Methods

Data Source and Preprocessing

PCL components were derived from the Traditional Chinese Medicine Integrated Database (TCMID, http://www.megabionet.org/tcmid/) and removed duplicates based on CAS Registry Number and PubChem CID (16). The SMILES format of PCL components was obtained from the PubChem (https://pubchem.ncbi.nlm.nih.gov/) database. The targets, possibly participated in PCL treating, were obtained from the Swiss Target Prediction (http://www.swisstargetprediction.ch/), and the cutoff was set probability > 0. The GeneCards (https://www.genecards.org/) database and the OMIM (https://www.omim.org/) database provided relative targets of pancreatic cancer. “Pancreatic Cancer” and “Homo sapiens” were set when searching for relative targets and then targets were standardized into gene symbols by R package: org.Hs.eg.db (17). The intersection of disease and compound targets was obtained and visualized as a Venn plot (18).

Construction of the Compound-Disease-Target Network

The overlapping targets of compounds and pancreatic cancer were integrated into Cytoscape V3.8.2 served as a platform for constructing the compound-disease-target network and visualizing the relationship among them (19). Network topological arguments such as “Degree”, “Closeness Centrality”, and “Betweenness Centrality” were calculated by undirected graph Analyze Network and used to screen active compounds with the median of abovementioned arguments setting as the optimal threshold.

Analysis of the Protein-Protein Interaction (PPI) and Expression Profile of Core Targets

Aiming to identify the core targets in the compound-disease-target network, the overlapping targets were analyzed by Cytoscape StringApp V1.6.0 based on the STRING database (https://string-db.org/) (20, 21). We constructed the PPI network based on “Homo sapiens” and “Highest confidence (0.900)”, and then identified the core targets ranked by topological arguments. The expression profile of core targets was performed between tumor and normal tissues on the basis of The Cancer Genome Atlas (TCGA) database and the Genotype-Tissue Expression (GTEx) database respectively.

Gene Ontology and Kyoto Encyclopedia Genes and Genomes Enrichment Analyses

We applied Gene Ontology (GO) functional enrichment and Kyoto Encyclopedia of Genes and Genomes (KEGG) pathway enrichment analyses to search biological function, cell location, and potential mechanisms by R package: clusterProfiler (22). The statistical significance threshold was set at P value < 0.01 and q value < 0.05. The outcome of GO and KEGG pathway enrichments were presented by R package: GOplot (23).

Prognostic Value of Core Targets for The Evaluation of Pancreatic Cancer

We used UCSC Xena to obtain gene expression and survival data of pancreatic cancer patients at TCGA and categorized the samples into high- (50%) and low- (50%) cohorts with the median of expression level as thresholds (24, 25). The multivariate Cox proportional hazards model was also performed to determine the independent prognostic value of core targets. P < 0.05 was considered the statistically significant difference. The correlation of core targets and immune infiltration was calculated based on the TIMER (https://cistrome.shinyapps.io/timer/) database (26).

Molecular Docking

Discovery Studio 4.5 client is a ligand-receptor docking software and widely used for estimating their complementarity by the scoring function. In the PDB database, the proper structures of core targets were searched and downloaded, which included the pleckstarin homology domain from human Akt (AKT1, PDB ID: 1H10), human Hsp90-alpha with 9-Butyl-8-(3,4,5-trimethoxy-benzyl)-9H-purin-6-ylamine (HSP90AA1, PDB ID: 1UY6), crystal structure of Fyn kinase domain complexed with staurosporine (FYN, PDB ID: 2DQ7), SH3 domain of human Lck (LCK, PDB ID: 2IIM), Lyn kinase domain (LYN, PDB ID: 3A4O), Crystal structure of human ERK2 complexed with a MAPK docking peptide (MAPK1, PDB ID: 4H3P), human Src A403T mutant bound to kinase inhibitor bosutinib (SRC, PDB ID: 4MXX), the E1-domain of the amyloid precursor protein (APP, PDB ID: 4PWQ), Stat3 Core in complex with compound SI109 (STAT3, PDB ID: 6NUQ), the compound bound to the PI3Ka catalytic subunit p110alpha (PIK3CA, PDB ID: 6OAC). We defined the active site based on co-crystallized ligands, removed water molecules, and added hydrogen atoms to macromolecules. In addition, the structures of active compounds were obtained from the PubChem database. We applied the CHARMm force field on the structures and minimized them to the closest local minimum. Subsequently, the active compounds were docked into receptors in the pattern of semi-flexible docking. The CDOCKER interaction energy is the scores of the ligand-receptor complex and normalized with Z-score in the matrix. The compound had the best conformations with proteins was considered a candidate and further studied in mice.

Cell Lines and Cell Culture

The murine pancreatic cancer cell line Panc 02 and mouse macrophage cell line RAW 264.7 cells were obtained from American Type Culture Collection and employed for the experiment. The cells were

incubated with Gibco Dulbecco's modified Eagle's medium with 100 μg/mL streptomycin and 100 U/mL penicillin and 10% fetal bovine serum (Biological Industries, Israel) in an incubator at 37°C and 5% CO_2.

Cell Proliferation Assay

According to the protocol, cell proliferation was monitored by the CCK-8 assay (Dojindo Laboratories, Kumamoto, Japan). Panc 02 cells were seeded in a 96-well plate and treated with different concentrations of IBC. After incubation for 24 h, the 10 μl of CCK-8 reagent was added and incubated for another 2 h at 37°C. Finally, the complex resolution was detected by a microplate at 450 nm.

Apoptosis and ROS Assay

After treatment with IBC (10 μM, 20 μM) for 24 h, Panc 02 cells were collected and stained with Annexin V and propidium iodide (PI) according to manufacturer's instructions (Tianjin Sungene Biotech, China). Meanwhile, Panc 02 cells were stained with DCFH-DA to detect the level of ROS generation. Both were identified by flow cytometry (ACEA, USA).

Orthotopic Model of Pancreatic Cancer

All animal experiments were reviewed and approved by the Medicine Ethical Committee of Tianjin Nankai Hospital. Orthotopic models of pancreatic cancer were established as described previously (27). Briefly, Panc 02 cells (5×10^5), resuspended in 50 μl PBS, were injected into the pancreas of female 6- to 8-week-old C57BL/6 mice (the Experimental Animal Center of Military Medical Sciences, Beijing, China) by insulin syringe. On the third day after the model was established, IBC (20 mg/kg/day) was administered intraperitoneal injection daily for 10 days.

Flow Cytometry

The tumor tissue was cut up with scissors and digested with enzymes for 30 minutes at 37°C, including 0.05 mg/mL of type-IV collagenase (Sigma, USA), DNase I (Sigma, USA), and hyaluronidase (Sigma, USA). The tumor tissue was ground into single cells through a 70 μm strainer. Tumor mononuclear cells were isolated by density gradient centrifugation, and the density gradient solution was 40% percoll and 80% percoll (GE, USA). The spleen tissue was ground into single cells through a 40 μm strainer (FALCON, USA). The further red blood cell lysate was used to remove blood cells. Tumor mononuclear cells and spleen cells were stained with the following antibodies: CD11b-FITC, Ly6G-PerCP, Ly6c-PE, CD4-APC, CD8-PE, NK1.1-PE, F4/80-APC, Gr-1-PE, and CD206-PE. NK Cells ($CD3^-NK1.1^+$), M-MDSC Cells ($Ly6C^+CD11b^+$), PMN-MDSC Cells ($Ly6G^+CD11b^+$), CD4 Cells ($CD3^+CD4^+$), CD8 Cells ($CD3^+CD8^+$), MDSCs cells ($CD11b^+Gr\text{-}1^+$), and M2 macrophage cells ($CD11b^+F4/80^+CD206^+$) were detected and analyzed by NovoCyte (ACEA, USA).

RNA extraction and real-time PCR

Total RNA was extracted from RAW264.7 cells by using Trizol reagent (Takara, Japan) according to the manufacturer's instructions. The mRNA was reverse transcribed into cDNA using cDNA Synthesis SuperMix (TransGen Biotech, China) and real-time PCR was carried out by using SYBR Green Master Mix (TransGen Biotech, China). Quantitative fluorescence analysis was performed using the ABI 7500 Real-time PCR System (Thermo Scientific, USA). GAPDH was used as an internal reference and relative target gene expression was calculated using the $2^{-\Delta\Delta Ct}$ method. The primer sequences used in this study were as follows: Arginase 1 (ARG1) (F) 5'-CTCCAAGCCAAAGTCCTTAGAG-3' and (R) 5'-GGAGCTGTCATTAGGGACATCA-3'; Mannose Receptor C-Type 1 (MRC1) (F) 5'-CTCTGTTCAGCTATTGGACGC-3' and (R) 5'-CGGAATTTCTGGGATTCAGCTTC-3'; GAPDH (F) 5'-ATGGTGAAGGTCGGTGTGAACG-3' and GAPDH (R) 5'- CGCTCCTGGAAGATGGTGATGG-3'; TGF-β (F) 5'-GGACCGCAACAACGCCATCTAT-3' and TGF-β (R) 5'- TTCAGCCACTGCCGTACAACTC-3'.

Isolation of bone marrow (BM) cells

The healthy C57BL/6 mice were separated and the two bone ends were cut off, and then Gibco Dulbecco's modified Eagle's medium with 100 μg/mL streptomycin and 100 U/mL penicillin was used to flush out the cells. BM-derived MDSCs were induced using 40 ng/mL GM-CSF (PeproTech, USA) and 40 ng/mL IL-6 (PeproTech, USA). At the same time, these cells were treated with IBC (10 μM) for 4 days.

Ki67 staining

The tumor tissues were fixed with 4% paraformaldehyde, embedded in paraffin, and made into 4-μm sections. Then the sections were incubated with primary antibodies for the proliferation marker protein Ki67 (anti-Ki67) (Cell Signaling Technology, Boston, USA). Subsequently, the section incubated with horseradish peroxidase-conjugated goat anti-rabbit immunoglobulin G (ZSJQB Co. Ltd, Beijing). Following incubation, hematoxylin was utilized to counterstain and the tissues were observed under the fluorescence inverted microscope.

Terminal deoxynucleotidyl transferase-mediated dUTP nick end labeling (TUNEL) staining

The tumor tissues were fixed with 4% paraformaldehyde, embedded in paraffin, and made into 4-μm sections. Then the sections were incubated with TUNEL reaction buffer according to the manufacturer's instructions (Yeasen Biotechnology, Shanghai). The nucleus was stained with DIPA for 5 min at room temperature without light and the sections were observed under the fluorescence inverted microscope.

Statistical Analysis

Statistical analysis was performed using R (version 4.03) and Rstudio software. Student's *t* test and one-way ANOVA were used to test the significance of differences in vivo and vitro assay. $P < 0.05$ was considered a gold standard of significant difference in this research.

Results

Data Source and Preprocessing

In this research, 36 compounds were initially obtained from TCMID. After removing 2 duplications and 6 compounds without any predicted targets, the integrated information of structures and predicted targets is shown in Table S1. Absorbed prototype compounds are the most pattern of TCM worked in vivo and therefore predicted to construct the network (28). In total, 479 targets of PCL were obtained by the Swiss Target Prediction database. Subsequently, the keywords, “Pancreatic Cancer”, were submitted to the OMIM and GeneCard database for searching relative targets, and 11489 targets were acquired. 412 overlapping targets between compounds and pancreatic cancer were considered as potential treatment targets and further analyzed (Fig. 2A).

Construction of the Compound-Disease-Target Network

The network consisted of 441 nodes (28 compounds nodes, 412 overlapping target nodes, 1 disease node) and 2296 edges (Fig. 2B). Larger nodes represent higher correlation and importance. The hub nodes were characterized by Degree ≥ 35, Betweenness Centrality ≥ 0.002, and Closeness Centrality ≥ 0.36, containing Bavachalcone, Bavachin, Bavachinin, Isobavachalcone, Isobavachin, Bakuchiol, Stearic acid, Isoneobavachalcone, Bakuchalcone, Backuchiol, Angelicin, Corylinal, and Corylin (Table S2). These compounds might be the active compounds of PCL in the treatment of pancreatic cancer.

Analysis of the PPI network and Expression Profile of Core Targets

We analyzed 412 overlapping targets and constructed the PPI network (Fig. 2C). The larger and redder the node, the stronger is the interaction. In total, 299 nodes and 1956 edges were calculated and ranked by topological arguments. The top 10 targets were considered core targets, including PIK3CA, SRC, MAPK1, AKT1, APP, STAT3, FYN, LCK, LYN, and HSP90AA1 (Table S2). Furthermore, the expression profile of 10 core targets in 182 tumor and 165 normal tissues is presented as a heatmap in Fig. 2D.

Gene Ontology and Kyoto Encyclopedia Genes and Genomes Enrichment Analyses

The top 30 GO terms are obtained and presented in Fig. 3A, consisting of 10 biological processes (BP), 10 cellular components (CC), and 10 molecular functions (MF) terms. The targets of BP terms mainly dealt with peptidyl-tyrosine phosphorylation, regulation of small molecule metabolic process, regulation of lipid metabolic process, peptidyl-tyrosine modification, protein autophosphorylation, and regulation of MAP kinase activity. The CC terms mainly included membrane raft, membrane microdomain, and membrane region. The results of MF terms showed that the targets were mainly connected with protein serine/threonine kinase activity, protein tyrosine kinase activity, nuclear receptor activity, ligand-activated transcription factor activity, and transmembrane receptor protein kinase activity. On the other hand, we obtained 143 KEGG pathway items and selected the top 10 pathways to visualize (Fig. 3B). The main pathways included PI3K-Akt signaling pathway, EGFR tyrosine kinase inhibitor resistance, Neuroactive ligand-receptor interaction, Sphingolipid signaling pathway, and Lipid and atherosclerosis.

Prognostic Value of Core Targets for the Evaluation of Pancreatic Cancer

As shown in Fig. 4, lowly expressed FYN ($P = 0.004$) and highly expressed MAPK1 ($P = 0.022$) are associated with poor prognosis, and the correlations of the other core targets and overall survival time are not tested for statistical significance ($P < 0.05$). Subsequently, the multivariate Cox regression model also revealed that FYN, MAPK1, and PIK3CA possessed the independent prognostic value in pancreatic cancer (Fig. 5A). The result of the TIMER database suggested that the expression level of FYN, MAPK, and PIK3CA correlate with immune infiltrates of B cell, $CD8^+$ cell, macrophage, neutrophil, and dendritic cell (Figs. 5B-D).

The Molecular Docking of Active Compounds and Core Targets

After screening above, 13 active compounds and 10 core targets were performed to dock, and the docking scores were normalized and visualized in Fig. 6A. We estimated the interaction between ligands and receptors based on the docking score, docking conformation, and key residues. IBC was considered a candidate and further studied its antitumor activity and underlying mechanisms. The conformations of 10 core targets for the IBC are presented in Fig. 6B.

Isobavachalcone inhibited cell proliferation and induced cell apoptosis of Panc 02 cells

To identify the biological role of IBC on pancreatic cancer, we put IBC with different concentrations into Panc 02 cells. CCK-8 assay demonstrated that IBC significantly inhibited the proliferation abilities of Panc 02 cells at 24 h relative to the control group (Figure S1A). Then, the cell apoptosis and ROS production of Panc 02 cells were tested by flow cytometry. Moreover, IBC treatment with various concentrations for 24h triggered cell apoptosis and ROS generation (Figures S1B-D). To determine the functional role of ROS in IBC-induced cell apoptosis, NAC, a ROS scavenger, was applied before IBC treatment. The results showed that NAC pretreatment abrogated IBC-induced apoptosis of Panc 02 cells. The results indicated that IBC could inhibit the proliferation and induce apoptosis of pancreatic cancer cells by increasing the production of ROS.

Isobavachalcone Suppressed Orthotopic Pancreatic Cancer in Mice

To further validate the role of IBC in pancreatic cancer, we established the orthotopic pancreatic cancer model in mice and treated them with IBC for 10 days. The tumor weight decreased significantly after IBC treatment at 10 days versus the control group (Figs. 7A-B). In addition, the results of immunohistochemistry for Ki67 staining showed that cell proliferation ability was suppressed by IBC in vivo (Figs. 7C and 7E). What is more, the immunofluorescence images with TUNEL staining showed the proportion of apoptotic cells was directly elevated by IBC in vivo (Figs. 7D and 7F).

Isobavachalcone inhibited the expansion of M2 macrophages and MDSCs in mice

In the tumor microenvironment, immunosuppressive cells such as M2 macrophages and MDSCs infiltrated and promoted tumor growth and metastasis (29). Therefore, we tested the effect of IBC in tumor tissues and spleen. The results showed that IBC could significantly reduce the accumulation of M2

macrophages in tumor tissue and spleen (Fig. 8A-D). In addition, IBC could significantly reduce the number of M2 macrophages in tumor tissue (Figure S2A). We used the polarization of RAW 264.7 cells and illustrated the mechanism of polarization in the presence or absence of IBC (10 μM). The result indicated that IBC inhibited the polarization of RAW 264.7 cells to M2 macrophages and reduced the expression of ARG1 and MRC1 (Figure S2B-E). Interestingly, IBC treatment also reduced the proportions of MDSCs in tumor tissue but not in spleens (Fig. 9A-D). Moreover, IBC could significantly reduce the M-MDSC and PMN-MDSC cells in the tumor tissues. Due to MDSCs mainly performing immunosuppressive functions by expressing ARG1 and TGF-β, we used GM-CSF and IL-6 to induce MDSCs from the BM of the mouse and validate the mRNA expression of ARG1 and TGF-β. The results showed that IBC inhibited the transcription of ARG1 and TGF-β in BM-derived MDSCs (Figure S3). These data suggested that IBC could attenuate the orthotopic pancreatic tumor in mice by inhibiting the expansion of M2 macrophages and MDSCs in the tumor tissue.

Isobavachalcone promoted the population of $CD8^+$ cells in mice

We evaluated the ratio of $CD4^+$, $CD8^+$, and NK cells in tumor tissues and spleen by flow cytometry to simultaneously examine the changes of the immune cell subsets. The results showed that IBC could significantly increase the accumulation of $CD8^+$ in tumor tissue and spleen (Fig. 9E-H). Whereas, the IBC treatment did not affect the frequencies of $CD4^+$ in tumor and spleen tissues. Furthermore, our results also did not reveal any changes in the NK cell populations of tumor and spleen tissues (Figure S4).

Discussion

As of 2021, partially as the aging population and improvement of treatments in other cancers, pancreatic cancer is increasing per year and perhaps going to be the second leading cause of cancer death (30). The main deficiency of the standard treatment is the high rate of primary irresectability and surgery complications (31). As a consequence, neoadjuvant concepts with antitumor drugs are positively used for pancreatic cancer. Although widespread efforts have been made to develop antitumor agents in pancreatic cancer, limited efficacy and tolerance have meant that searching for a new nature compound with potent and alternative antitumor activity is imperative (32).

In this research, PCL components were obtained from the TCMID database and then submitted to Swiss Target Prediction for potential targets. The relative targets of pancreatic cancer were retrieved from the GeneCard and OMIM database. Subsequently, we found 412 overlapping targets in common and constructed a compound-disease-target network. Ranked by topological arguments, 13 compounds were considered active compounds. We also constructed the PPI network and identified the top 10 core targets. The expression profile of 10 core targets in 182 tumor and 165 normal tissues were visualized as a heatmap to observe the distribution. The GO and KEGG pathway analyses were performed to assess the 412 overlapping targets. Based on the GO enrichment map, we made the following observations: the BP terms were mainly concerned with tyrosine modification, metabolic process, and regulating MAP kinase activity; the CCs were mainly involved with various cell membranes such as presynaptic membrane and

synaptic membrane; the MFs mainly dealt with numerous protein kinase activity and drug binding. The result of KEGG pathway analysis was summarized in the PI3K-Akt signaling pathway, EGFR tyrosine kinase inhibitor resistance, Neuroactive ligand-receptor interaction, Sphingolipid signaling pathway, and Lipid and atherosclerosis.

In addition, the correlation of 10 core targets and the patient prognosis was confirmed by survival analysis and multivariate Cox regression model. The results showed that MAPK1, FYN, and PIK3CA could be considered independent prognostic factors, but PIK3CA had no significant influence on the overall survival time of patients ($P = 0.16$). MAPK1 plays a vital role in the tumor microenvironment among various cancers. In head and neck squamous cell carcinoma, MAPK1 is upregulated in vivo and vitro and highly correlated with recurrence via regulating the tumor microenvironment (33). Secreted exosomal CMTM6 of oral squamous cell carcinoma induces M2-like macrophages polarization and promotes malignant progression via the ERK1/2 signaling pathway (34). Among ovarian cancer patients, FYN is one of the indispensable kinase targets of CXC chemokines which activate the downstream signaling pathways to influence tumor progression (35). Thus, the correlation of 3 independent factors and immune infiltration was investigated in the TIMER database. It was suggested that FYN, MAPK, and PIK3CA were positively correlated with immune infiltration of B cell, $CD8^+$ cell, macrophage, neutrophil, and dendritic cell. After the above analysis, the 10 core targets were credible and set as receptors to dock with 13 active compounds of PCL. Figure 5 demonstrated that IBC possessed the best conformations and docking scores with 10 core targets. Therefore, we considered IBC as a candidate compound and further studied antitumor ability and influence on the immunosuppressive tumor microenvironment of pancreatic cancer.

Our study showed that IBC could inhibit proliferation of Panc 02, promote cell apoptosis via increasing the level of ROS production, and attenuate weights of orthotopic cancer by inhibiting tumor proliferation and increasing tumor apoptosis directly, which is in line with the previous studies (12, 13, 36). Furthermore, we focused on the effects of IBC treatment in the tumor microenvironment of pancreatic cancer. The formation of the tumor microenvironment, induced by interactions between pancreatic epithelial/cancer cells and stromal cells, contributes to desmoplasia and immunosuppression and is always accompanied by poor prognosis (37). M2 macrophages and MDSCs play a significant role in the immunosuppressive tumor microenvironment and are considered obstacles in immunotherapy (38).

M2 macrophages, one of the critical components of the tumor microenvironment, highly accumulate in tumor tissues and participate in cancer progression, simultaneous immunosuppression, angiogenesis, and drug resistance (39, 40). Our data revealed that both M2 macrophages in tumor tissues and spleen significantly decreased administrated by IBC. Thus, IBC could serve as an antitumor agent on pancreatic cancer by regulating M2 macrophages polarization. The potential mechanisms might be related to MAPK1, FYN, and PIK3CA and will be verified in the following experiment.

MDSCs, a heterogeneous group of immune cells, are derived from the bone marrow and transfer the solid tumor and peripheral lymphoid organs to contribute to the formation of the tumor microenvironment (41).

Along with inherent immunosuppressive activity, it can amplify the function of macrophages and dendritic cells and promote carcinoma progression via cell-cell interaction (42). In this research, it was found that a reduction of MDSCs in tumor tissues, in which IBC could significantly improve the immunosuppressive tumor microenvironment via inhibiting the mRNA expression of ARG1 and TGF-β. However, the proportion of MDSCs in the spleen has no change. The result indicated that the function and fate of MDSCs remain different in the tumor and peripheral lymphoid organs of pancreatic cancer.

$CD8^+$ cells and NK cells exert the direct antitumor effect and play important roles in the anti-tumor immune response. In this research, it was found that a reduction of $CD8^+$ in tumor and spleen tissues, in which IBC could significantly improve the immunosuppressive tumor microenvironment via increasing the proportion of $CD8^+$ cells. However, the proportion of NK cells has not changed. Thus, IBC could serve as an antitumor agent on pancreatic cancer by regulating the proportion of $CD8^+$ cells.

Conclusions

In summary, we demonstrated that IBC treatment inhibits Panc 02 cell proliferation, promotes cell apoptosis via increasing production of ROS, and activates antitumor immunity. This provides a new approach to elucidate the antitumor activity of IBC and could serve as a reference for the treatment of the immunosuppressive tumor microenvironment in pancreatic cancer.

Declarations

Conflict of Interest

The authors declare that the research was conducted in the absence of any commercial or financial relationships that could be construed as a potential conflict of interest.

Author Contributions

YW, DHL, and LY designed the study; XML completed the part of bioinformatics. HBZ collected the data. JLC, YZZ, and JHJ performed the experimental validation. QYG and XFY participated in the annotation and manuscript. All authors read and approved the final manuscript.

Funding

The present study was supported by the National Natural Science Foundation of China (No. 81602773), Tianjin Natural Science Foundation Youth Fund (No. 19JCZDJC33100; 18JCQNJC13400), and the science foundation of Tianjin Municipal Health Bureau (No. 2019038; No. 2019050).

Acknowledgments

We would like to thank all persons who participated in the study.

References

1. Ilic M, Ilic I. Epidemiology of pancreatic cancer. World J Gastroenterol. 2016;22(44):9694–705.
2. Dreyer SB, Chang DK, Bailey P, Biankin AV. Pancreatic Cancer Genomes: Implications for Clinical Management and Therapeutic Development. Clinical cancer research: an official journal of the American Association for Cancer Research. 2017;23(7):1638–46.
3. Wu D, Li X, Zhang X, Han F, Lu X, Liu L, et al. Pharmacometabolomics Identifies 3-Hydroxyadipic Acid, d-Galactose, Lysophosphatidylcholine (P-16:0), and Tetradecenoyl-l-Carnitine as Potential Predictive Indicators of Gemcitabine Efficacy in Pancreatic Cancer Patients. Frontiers in oncology. 2019;9:1524.
4. Karamitopoulou E. Tumour microenvironment of pancreatic cancer: immune landscape is dictated by molecular and histopathological features. British journal of cancer. 2019;121(1):5–14.
5. Martinez-Bosch N, Vinaixa J, Navarro P. Immune Evasion in Pancreatic Cancer: From Mechanisms to Therapy. Cancers. 2018;10(1).
6. Masucci MT, Minopoli M, Carriero MV. Tumor Associated Neutrophils. Their Role in Tumorigenesis, Metastasis, Prognosis and Therapy. Frontiers in oncology. 2019;9:1146.
7. Gun SY, Lee SWL, Sieow JL, Wong SC. Targeting immune cells for cancer therapy. Redox biology. 2019;25:101174.
8. Yan DM, Chang YX, Wang YF, Liu EW, Li J, Kang LY, et al. In vivo pharmacokinetics of bakuchiol after oral administration of bakuchiol extraction in rat plasma. J Ethnopharmacol. 2010;128(3):697–702.
9. Zhou L, Tang J, Yang X, Dong H, Xiong X, Huang J, et al. Five Constituents in Psoralea corylifolia L. Attenuate Palmitic Acid-Induced Hepatocyte Injury via Inhibiting the Protein Kinase C-α/Nicotinamide-Adenine Dinucleotide Phosphate Oxidase Pathway. Front Pharmacol. 2019;10:1589.
10. Alam F, Khan GN, Asad M. Psoralea corylifolia L: Ethnobotanical, biological, and chemical aspects: A review. Phytotherapy research: PTR. 2018;32(4):597–615.
11. Kuete V, Sandjo LP. Isobavachalcone: an overview. Chinese journal of integrative medicine. 2012;18(7):543–7.
12. Li Y, Qin X, Li P, Zhang H, Lin T, Miao Z, et al. Isobavachalcone isolated from Psoralea corylifolia inhibits cell proliferation and induces apoptosis via inhibiting the AKT/GSK-3β/β-catenin pathway in colorectal cancer cells. Drug design, development and therapy. 2019;13:1449–60.
13. Li K, Zheng Q, Chen X, Wang Y, Wang D, Wang J. Isobavachalcone Induces ROS-Mediated Apoptosis via Targeting Thioredoxin Reductase 1 in Human Prostate Cancer PC-3 Cells. Oxidative medicine and cellular longevity. 2018;2018:1915828.
14. Nishimura R, Tabata K, Arakawa M, Ito Y, Kimura Y, Akihisa T, et al. Isobavachalcone, a chalcone constituent of Angelica keiskei, induces apoptosis in neuroblastoma. Biol Pharm Bull. 2007;30(10):1878–83.
15. Yang L, Song L, Zhao S, Ma C, Wu D, Wu YL. Isobavachalcone reveals novel characteristics of methuosis-like cell death in leukemia cells. Chemico-biological interactions. 2019;304:131–8.

16. Huang L, Xie D, Yu Y, Liu H, Shi Y, Shi T, et al. TCMID 2.0: a comprehensive resource for TCM. Nucleic Acids Res. 2018;46(D1):D1117-d20.
17. Carlson M. org.Hs.eg.db: Genome wide annotation for Human. 2020.
18. Chen H. VennDiagram: Generate High-Resolution Venn and Euler Plots. 2018.
19. Shannon P, Markiel A, Ozier O, Baliga NS, Wang JT, Ramage D, et al. Cytoscape: a software environment for integrated models of biomolecular interaction networks. Genome Res. 2003;13(11):2498–504.
20. Doncheva NT, Morris JH, Gorodkin J, Jensen LJ. Cytoscape StringApp: Network Analysis and Visualization of Proteomics Data. J Proteome Res. 2019;18(2):623–32.
21. Szklarczyk D, Gable AL, Nastou KC, Lyon D, Kirsch R, Pyysalo S, et al. The STRING database in 2021: customizable protein-protein networks, and functional characterization of user-uploaded gene/measurement sets. Nucleic Acids Res. 2021;49(D1):D605-d12.
22. Yu G, Wang LG, Han Y, He QY. clusterProfiler: an R package for comparing biological themes among gene clusters. Omics. 2012;16(5):284–7.
23. Walter W, Sánchez-Cabo F, Ricote M. GOplot: an R package for visually combining expression data with functional analysis. Bioinformatics. 2015;31(17):2912–4.
24. Wang Y, Zhang Y, Wang Y, Shu X, Lu C, Shao S, et al. Using Network Pharmacology and Molecular Docking to Explore the Mechanism of Shan Ci Gu (Cremastra appendiculata) Against Non-Small Cell Lung Cancer. Front Chem. 2021;9:682862.
25. Goldman MJ, Craft B, Hastie M, Repečka K, McDade F, Kamath A, et al. Visualizing and interpreting cancer genomics data via the Xena platform. Nat Biotechnol. 2020;38(6):675–8.
26. Li T, Fan J, Wang B, Traugh N, Chen Q, Liu JS, et al. TIMER: A Web Server for Comprehensive Analysis of Tumor-Infiltrating Immune Cells. Cancer Res. 2017;77(21):e108-e10.
27. Xi Q, Zhang J, Yang G, Zhang L, Chen Y, Wang C, et al. Restoration of miR-340 controls pancreatic cancer cell CD47 expression to promote macrophage phagocytosis and enhance antitumor immunity. Journal for immunotherapy of cancer. 2020;8(1).
28. Tong H, Yu M, Fei C, Ji D, Dong J, Su L, et al. Bioactive constituents and the molecular mechanism of Curcumae Rhizoma in the treatment of primary dysmenorrhea based on network pharmacology and molecular docking. Phytomedicine. 2021;86:153558.
29. Lorenzo-Sanz L, Muñoz P. Tumor-Infiltrating Immunosuppressive Cells in Cancer-Cell Plasticity, Tumor Progression and Therapy Response. Cancer microenvironment: official journal of the International Cancer Microenvironment Society. 2019;12(2–3):119–32.
30. Neoptolemos JP, Kleeff J, Michl P, Costello E, Greenhalf W, Palmer DH. Therapeutic developments in pancreatic cancer: current and future perspectives. Nature reviews Gastroenterology & hepatology. 2018;15(6):333–48.
31. Heinrich S, Lang H. Neoadjuvant Therapy of Pancreatic Cancer: Definitions and Benefits. International journal of molecular sciences. 2017;18(8).

32. Zeng S, Pöttler M, Lan B, Grützmann R, Pilarsky C, Yang H. Chemoresistance in Pancreatic Cancer. International journal of molecular sciences. 2019;20(18).
33. Watermann C, Pasternack H, Idel C, Ribbat-Idel J, Brägelmann J, Kuppler P, et al. Recurrent HNSCC Harbor an Immunosuppressive Tumor Immune Microenvironment Suggesting Successful Tumor Immune Evasion. Clinical cancer research: an official journal of the American Association for Cancer Research. 2021;27(2):632–44.
34. Pang X, Wang SS, Zhang M, Jiang J, Fan HY, Wu JS, et al. OSCC cell-secreted exosomal CMTM6 induced M2-like macrophages polarization via ERK1/2 signaling pathway. Cancer immunology, immunotherapy: CII. 2021;70(4):1015–29.
35. Jin Y, Lin Q, Fei H, Xue L, Li L, Xi Q, et al. Bioinformatics Analysis of Potential Therapeutic Targets and Prognostic Biomarkers amid CXC Chemokines in Ovarian Carcinoma Microenvironment. Journal of oncology. 2021;2021:8859554.
36. Jing H, Zhou X, Dong X, Cao J, Zhu H, Lou J, et al. Abrogation of Akt signaling by Isobavachalcone contributes to its anti-proliferative effects towards human cancer cells. Cancer Lett. 2010;294(2):167–77.
37. Ren B, Cui M, Yang G, Wang H, Feng M, You L, et al. Tumor microenvironment participates in metastasis of pancreatic cancer. Molecular cancer. 2018;17(1):108.
38. Groth C, Hu X, Weber R, Fleming V, Altevogt P, Utikal J, et al. Immunosuppression mediated by myeloid-derived suppressor cells (MDSCs) during tumour progression. British journal of cancer. 2019;120(1):16–25.
39. Zhao S, Mi Y, Guan B, Zheng B, Wei P, Gu Y, et al. Tumor-derived exosomal miR-934 induces macrophage M2 polarization to promote liver metastasis of colorectal cancer. Journal of hematology & oncology. 2020;13(1):156.
40. Qian BZ, Pollard JW. Macrophage diversity enhances tumor progression and metastasis. Cell. 2010;141(1):39–51.
41. Kumar V, Patel S, Tcyganov E, Gabrilovich DI. The Nature of Myeloid-Derived Suppressor Cells in the Tumor Microenvironment. Trends in immunology. 2016;37(3):208–20.
42. Ostrand-Rosenberg S, Sinha P, Beury DW, Clements VK. Cross-talk between myeloid-derived suppressor cells (MDSC), macrophages, and dendritic cells enhances tumor-induced immune suppression. Semin Cancer Biol. 2012;22(4):275–81.

Supplementary

Tables S1-S2 are not available with this version

Figures

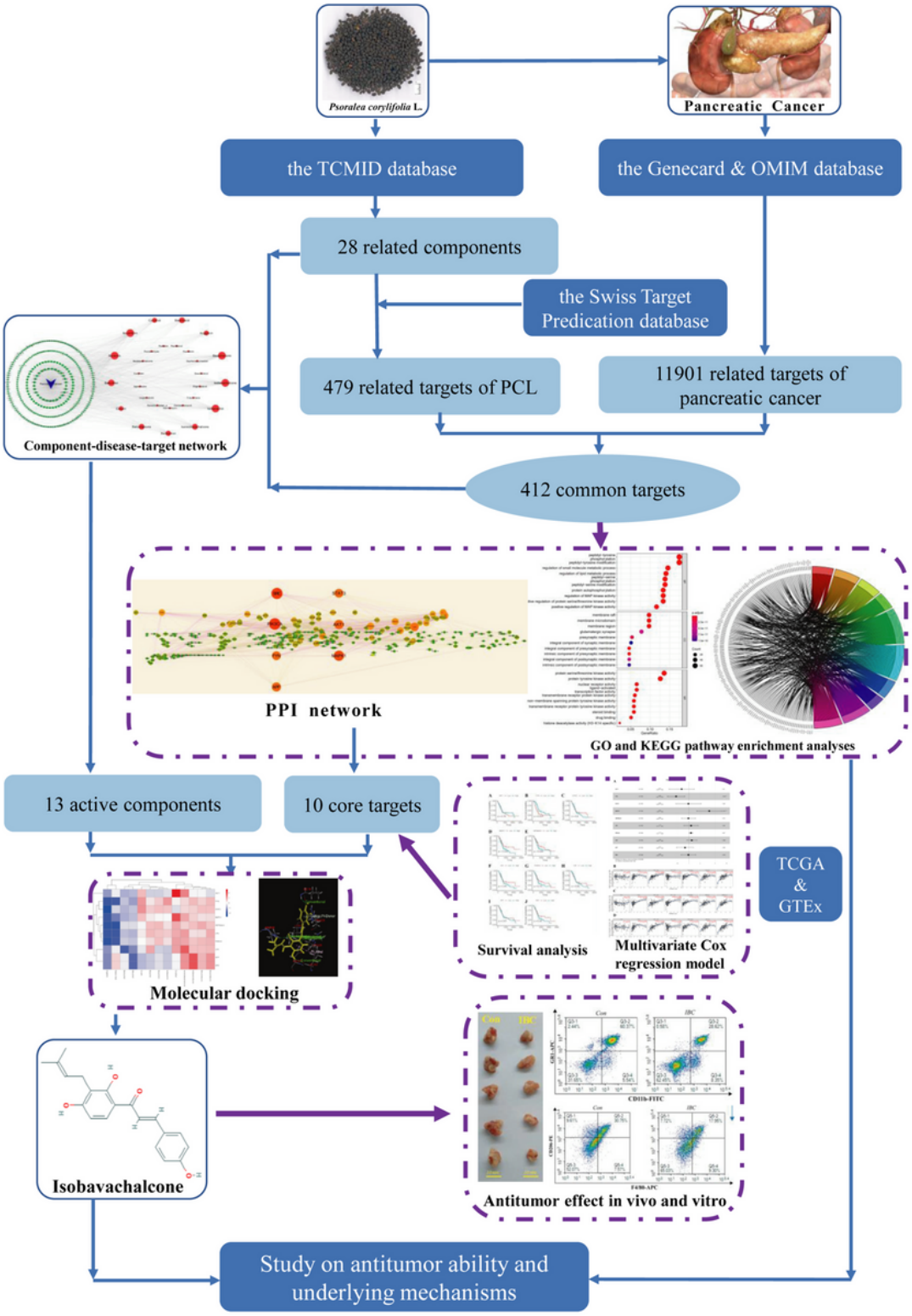


Figure 1

Research procedures used in the experiment to search for a candidate antitumor agent and invest the underlying mechanisms.

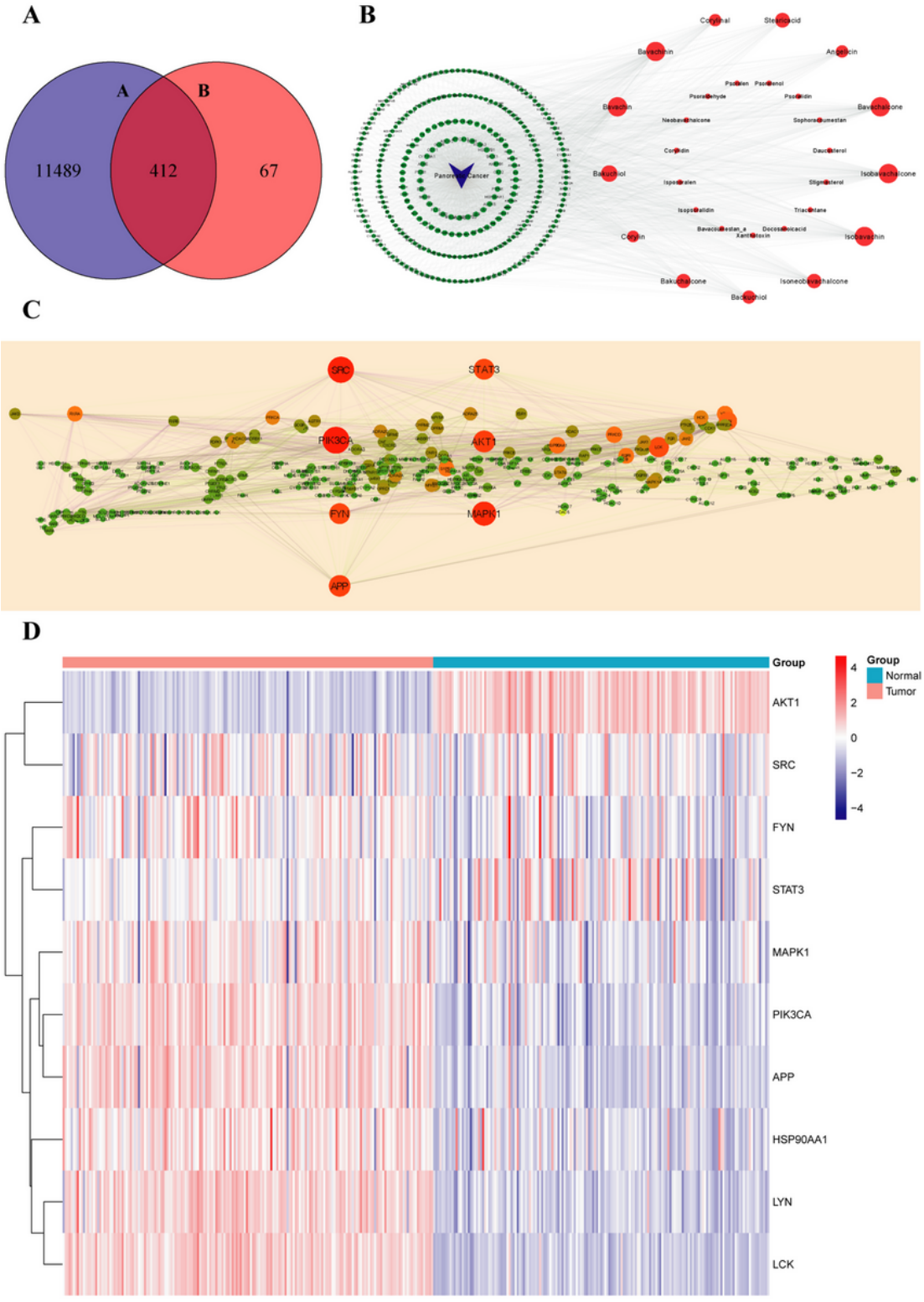


Figure 2

(A) Overlapping targets of PCL and pancreatic cancer. (A) 11901 targets of pancreatic cancer. (B) 479 targets of PCL components. **(B)** Compound-disease-target network (Red nodes represent PCL components, green nodes represent targets of pancreatic cancer, and blue nodes represent pancreatic cancer. The larger the node, the more important is the node in the network). **(C)** Protein-protein-interaction network of overlapping targets (The larger and redder node, the more important is the node in the

network). **(D)** Expression profile of the 10 core targets between the normal and tumor tissues (blue: low expression level; red: high expression level).

Figure 3

(A) Secondary classification dot plot of GO functional enrichment analysis including biological process (BP), cellular components (CC), and molecular function (MF). The abscissa shows the GO term, and the ordinate shows the numbers of genes enriched in the GO term. **(B)** Chord graph of the KEGG pathway enrichment analysis results. The different colors represent pathway terms, and the angle of the chord represents the numbers of genes enriched in the pathway term.

Figure 4

Survival analysis for 10 core targets. Orange lines represent sample groups with low gene expression, while green lines represent sample groups with high gene expression. **(A)** AKT1, **(B)** FYN, **(C)** STAT3, **(D)** MAPK1, **(E)** HSP90AA1, **(F)** LYN, **(G)** PIK3CA, **(H)** LCK, **(I)** APP, **(J)** SRC.

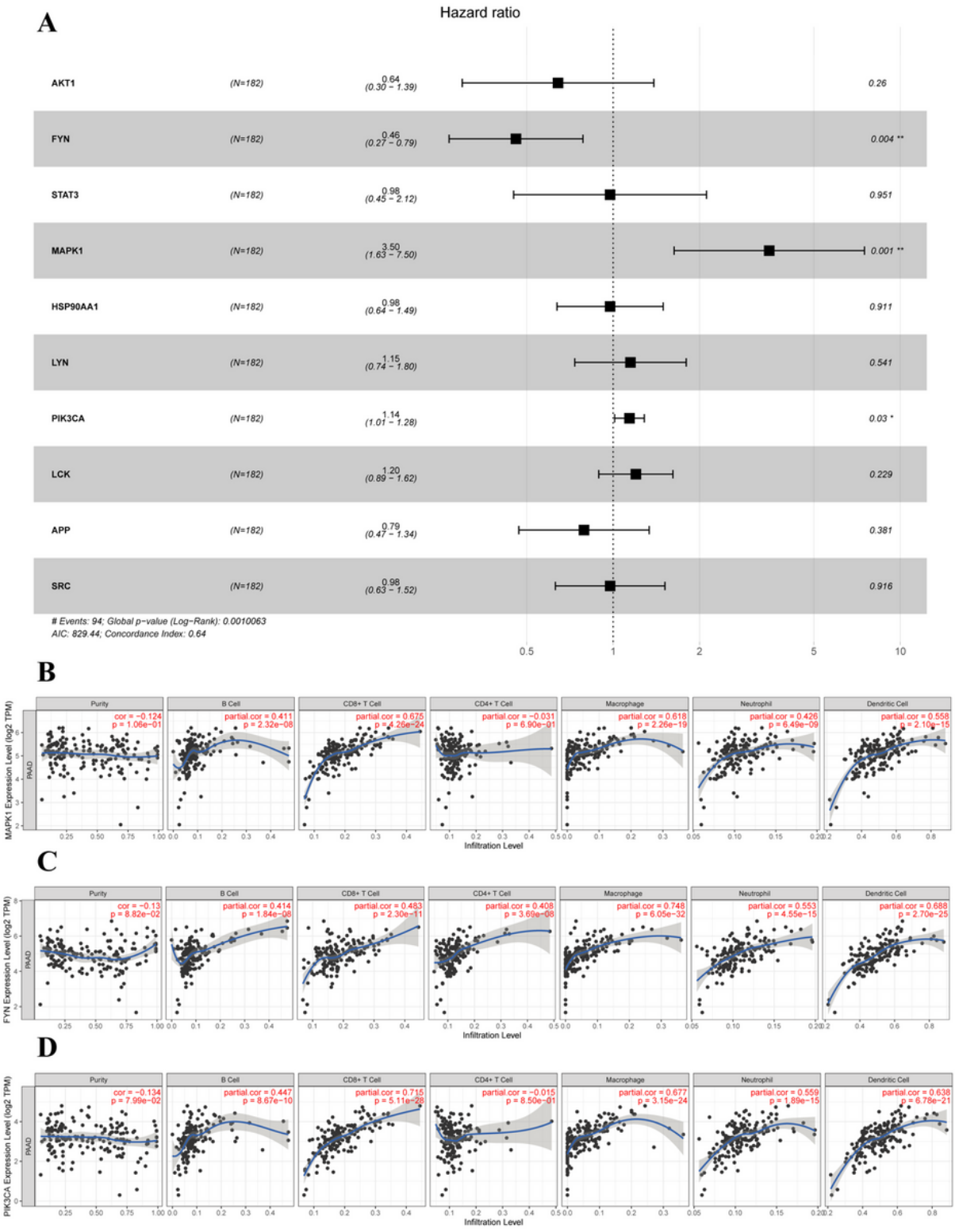


Figure 5

(A) Multivariate Cox regression model was performed to study the correlation of 10 core targets and patient survival. The model was analyzed by the Likelihood Ratio test, the Wald test, and the Logrank test, **P* < 0.05, ***P* < 0.001. **(B-D)** The correlations of targets expression level and immune cells infiltration (Purity, B Cell, $CD8^+$ Cell, $CD4^+$ Cell, Macrophage, Neutrophil, and Dendritic Cell).

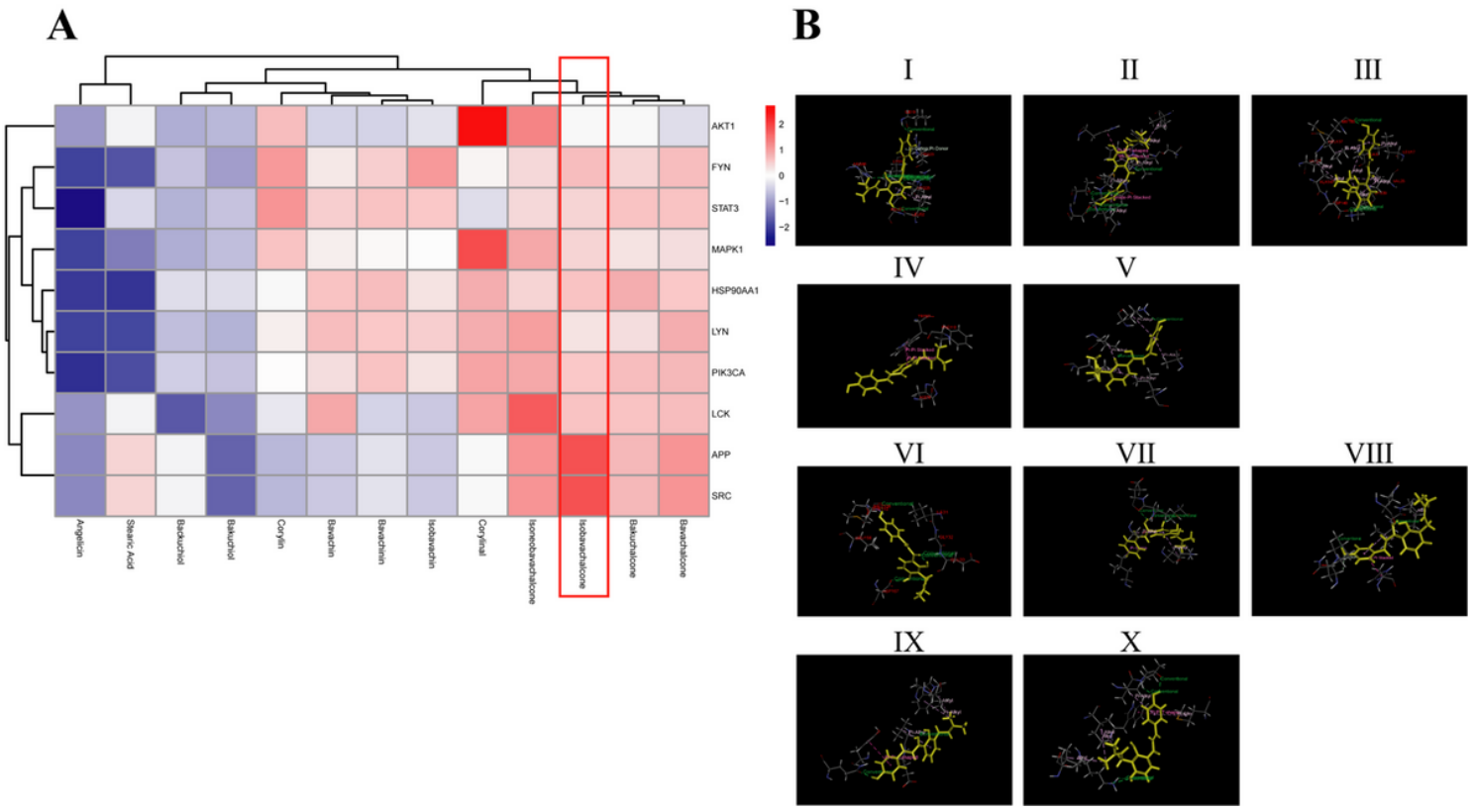


Figure 6

Matrix of molecular docking scores. **(A)** Heatmap of the CDOCKER interaction energy of 13 active compounds and 10 core targets after the Euclidean normalizing. **(B)** The docked conformation between IBC and 10 core targets. (Ⅰ) AKT1, (Ⅱ) HSP90AA1, (Ⅲ) FYN, (Ⅳ) LCK, (Ⅴ) LYN, (Ⅵ) MAPK1, (Ⅶ) SRC, (Ⅷ) APP, (Ⅸ) STAT3, (Ⅹ) PIK3CA.

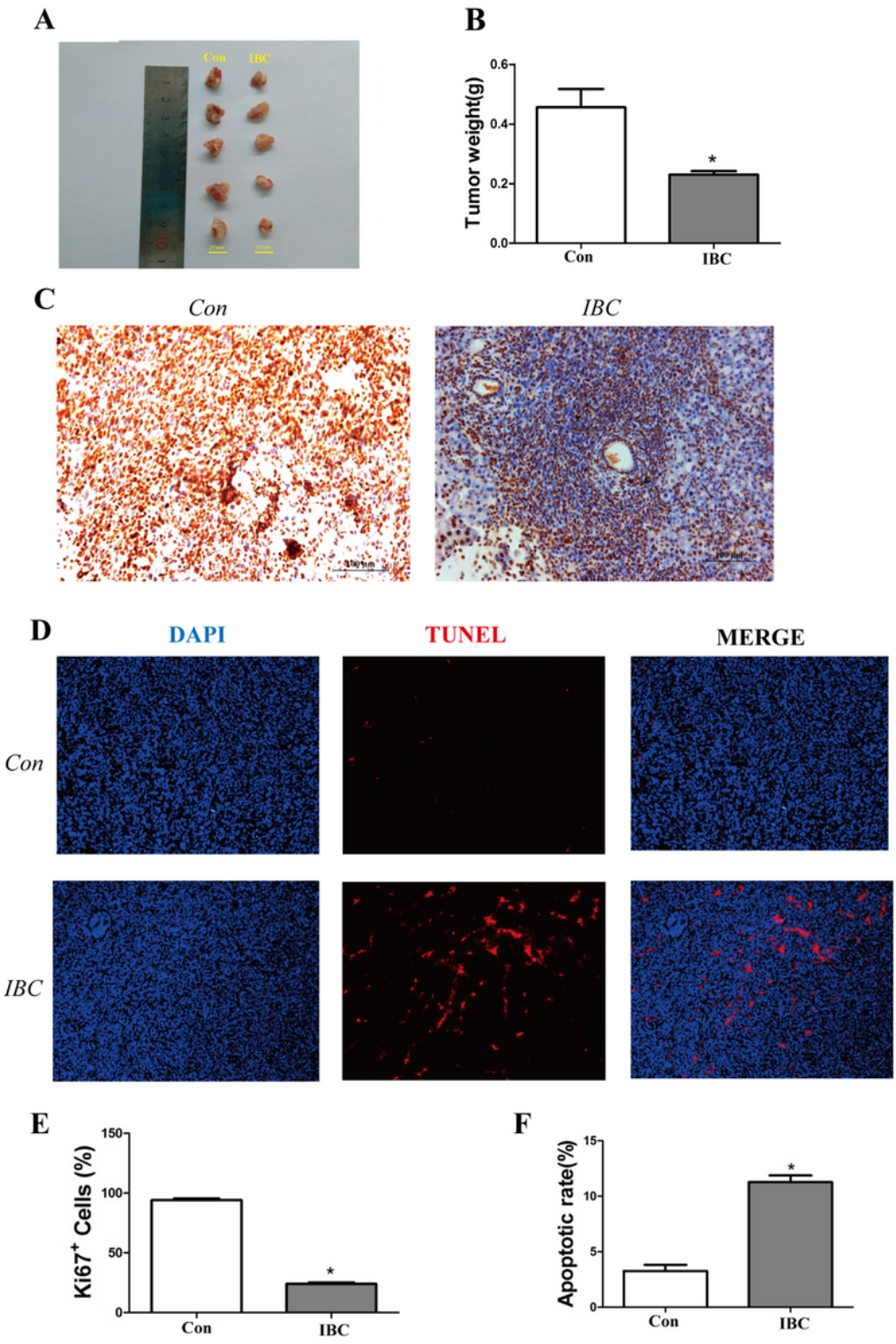


Figure 7

(A-B) The tumor tissues were isolated from the orthotopic models ($N = 5$). The therapeutic mice with orthotopic pancreatic tumors were treated IBC (20 mg/kg) for 10d. The columns represent the mean ± SEM. Student's *t* test was applied to analyze the data, $*P < 0.05$ versus the control. **(C)** The expression of Ki67 in tissues was valued through immunohistochemistry (scale: 100 μm). **(D)** TUNEL staining showed the proportion of apoptotic cells in tissues (scale: 100 μm). **(E)** Quantitative analysis of the $Ki67^+$ cells in

tumor tissues, *P < 0.05 versus the control. **(F)** Quantitative analysis of the apoptosis rate in tumor tissues, *P < 0.05 versus the control.

Figure 8

(A-B) The M2 macrophages polarized in the tumor tissue (N = 5), *P < 0.05 versus the control. **(C-D)** The M2 macrophages polarized in the spleen (N = 5), *P < 0.05 versus the control.

Figure 9

(A-B) In tumor tissues, the representative image of MDSCs proportion was reported. The columns represent the mean ± SEM. Student's *t* test was applied to analyze the data, *P < 0.05 versus the control. **(C-D)** The proportion of MDSCs in the spleen was reported, *P < 0.05 versus the control. **(E-F)** In tumor tissues, the representative image of $CD8^+$ proportion was reported. The columns represent the mean ± SEM. Student's *t* test was applied to analyze the data, *P < 0.05 versus the control. **(G-H)** The proportion of $CD8^+$ in the spleen was reported, *P < 0.05 versus the control.

Supplementary Files

This is a list of supplementary files associated with this preprint. Click to download.

- Figures1s4.docx